Computation of Resonant Frequencies of Cylindrical Ferrite Resonators Using GIBC's

Myung Jin Kong and Benjamin Beker

***Abstract*—A computational approach for resonant frequencies of cylindrical substrate-mounted resonators is presented in this paper. The resonator is made of ferrite material, which is magnetically anisotropic and characterized by a Hermitian tensor. It is mounted on top of a grounded dielectric substrate, and the entire assembly is covered with a tuning plate, leaving the sidewalls open. The generalized impedance boundary conditions (GIBC's) are derived for the ferrite material and are used to formulate the approximate solution to the boundary-value problem. The resulting transcendental equations are solved numerically, and variations of the resonant frequency with respect to bias field, magnetization, and dimensions of the structure are reported.**

***Index Terms*—Cylindrical resonators, ferrites, GIBC's.**

I. Introduction

Early microwave communication systems made wide use of metallic waveguides as filter elements. With the advent of microwave integrated circuit (MIC) technology, bulky waveguide filters were replaced with smaller microstrip-type circuit elements. Microwave characteristics of numerous microstrip-line integrated circuits (IC's) were studied extensively, even though they suffer from relatively low efficiency. Unlike MIC-type filters, dielectric resonators are commonly used to realize bandpass or band-reject filters at microwave frequencies with fairly high efficiency [1]. They are easy to manufacture, light weight, fairly small in size, and have high Q's. All these properties make them popular in microwave applications.

Typical materials that are used to make many resonators are high dielectric-constant ceramics, which can exhibit uniaxial anisotropy. The analysis of isolated isotropic resonators or those placed in a practical circuit environment is fairly extensive, ranging from analytic to general numerical methods [2]–[8]. On the other hand, only a limited amount of work on anisotropic resonators has been reported to date [9], though the finite-difference time-domain (FDTD) approach presented in [8] can also be applied to electrically and magnetically biaxial materials.

This paper describes the analysis of cylindrical resonators that are made of ferrites, which are characterized by Hermitian permeability tensors [10]. It exploits generalized impedance boundary conditions (GIBC's) that were originally proposed in [11] and later implemented for isotropic dielectric resonators in [7]. GIBC's are used to simplify the boundary-value problem, making it possible to derive a transcendental equation for the axial dependence of the fields. The analysis is restricted to the approximate dominant quasi-TE mode of the cylindrical resonator, though this approach is valid for other modes as well. The radiation modes are neglected, since the structure is partially shielded and, hence, their contributions are small [7]. The proposed approach is validated for the same approximate quasi-TE modes of a ferrite post sandwiched between two infinitely large perfectly conducting planes. Numerical data are provided showing the dependence of the resonant frequency of the substrate-mounted ferrite resonator as a function of applied biasing field, magnetization, and structural dimensions.

Manuscript received July 22, 1997; revised March 9, 1998.

The authors are with the Department of Electrical and Computer Engineering, University of South Carolina, Columbia, SC 29208 USA.

Publisher Item Identifier S 0018-9480(98)07234-2.

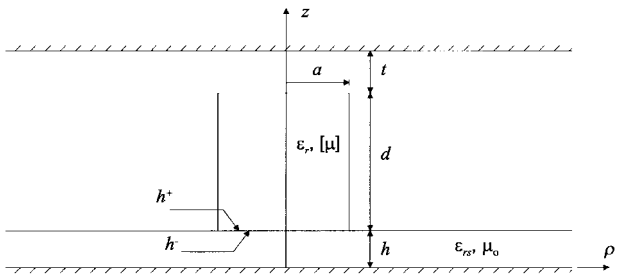

Fig. 1. Geometry of the substrate-mounted ferrite resonator.

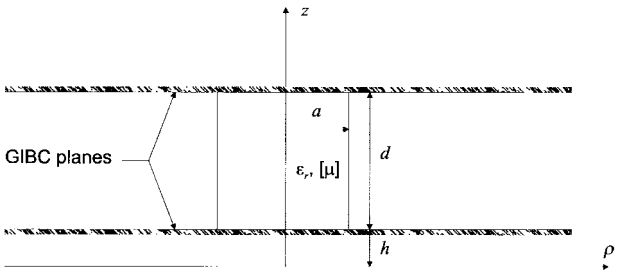

Fig. 2. Geometry of the equivalent boundary-value problem after application of GIBC's.

II. Formulation of the Boundary-Value Problem

Consider a cylindrical resonator (shown in Fig. 1), which is mounted on a grounded dielectric substrate and is covered with a metallic tuning plate. The resonator is composed of ferrite, which is characterized by a Hermitian permeability tensor ($[\mu]$) and a scalar dielectric constant (ε_r). The biasing field is assumed to be z-directed, which leads to the presence of xy–yx off-diagonal elements in $[\mu]$. Though this structure is highly symmetric and conforms well to the cylindrical coordinate system, exact analytical solution of this problem is very difficult. The difficulties stem from the need to enforce the boundary conditions at $z = h$ and $h + d$ in the radial plane of the geometry.

If well-defined boundary conditions at these two planes were known (e.g., for a resonating post placed between two metallic planes), then the analytical solution to this problem would become straightforward. The use of GIBC's permits a reduction of a complex problem (shown in Fig. 1) to a simpler problem (shown in Fig. 2). GIBC's provide for the boundary conditions at $z = h$ and $h+d$, which take into account the presence of the grounded substrate and tuning plate. Note that the boundary conditions are only needed for the axial components of the fields (E_z, H_z) since the transverse components can be expressed in terms of E_z and H_z. As it is well known that a dominant mode of operation for the circular resonator is of the quasi-TE type $(E_z \approx 0)$ [12], all subsequent analyses will be restricted to only this field distribution. In addition, unlike the work on GIBC's for isotropic dielectrics presented in [7], the procedure for deriving them for ferrites is presently unavailable and, hence, will be presented below.

To that end, the boundary conditions on H_z at the end caps of the resonator must be obtained first. This can be achieved by

expanding the tangential components of the E-field at the surface of the metal in Taylor series and relating them to H_z at $z = h^-$ and $z = (h+d)^+$. As shown in [7], E_x and E_y, which are zero at $z = 0$ and $z = (h+d+t)$, can be expanded in terms of Taylor series. The odd and even derivatives in this expansion are kept separately since the procedure for obtaining them is not the same.

The boundary condition for the odd derivatives of H_z at $z = h$ can be obtained from the x- and y-components of Faraday's law as follows:

$$\left(\frac{\partial E_z}{\partial y} - \frac{\partial E_y}{\partial z}\right)_{\left\{\begin{smallmatrix} h- \\ h+ \end{smallmatrix}\right\}} = -j\omega \begin{Bmatrix} (\mu_0 H_x)_{h-} \\ (\mu H_x + j\kappa H_y)_h \end{Bmatrix} \quad (1)$$

$$\left(\frac{\partial E_x}{\partial z} - \frac{\partial E_z}{\partial x}\right)_{\left\{\begin{smallmatrix} h- \\ h+ \end{smallmatrix}\right\}} = -j\omega \begin{Bmatrix} (\mu_0 H_y)_{h-} \\ (-j\kappa H_x + \mu H_y)_{h+} \end{Bmatrix}. \quad (2)$$

In the above equations, the permeability tensor $[\mu]$ has the following form:

$$[\mu] = \begin{bmatrix} \mu & j\kappa & 0 \\ -j\kappa & \mu & 0 \\ 0 & 0 & \mu_0 \end{bmatrix} \quad (3)$$

whose elements and a way to measure them are given in [10] and [13], respectively.

The next step is to express the z-derivatives of E_x and E_y just within the substrate ($z = h^-$) in terms of fields just within the resonator ($z = h^+$). This is accomplished by taking into account the fact that for the quasi-TE mode $E_z \approx 0$, and that H_x and H_y must be continuous at $z = h$ (or $z = h^{\pm}$). With this information, (1) and (2) can be rearranged, leading to

$$\begin{Bmatrix} \dfrac{\partial E_x}{\partial z} \\ \dfrac{\partial E_y}{\partial z} \end{Bmatrix}_{h-} \approx \frac{\mu_0}{\mu} \begin{Bmatrix} \dfrac{\partial E_x}{\partial z} + \omega\kappa H_x \\ \dfrac{\partial E_y}{\partial z} + \omega\kappa H_y \end{Bmatrix}_{h+}. \quad (4)$$

Note that the above expressions are only approximate equalities due to the assumed quasi-TE modal field distribution. However, for the sake of clarity, they will be replaced with equalities in a subsequent discussion.

To complete the derivation of the relationship between the odd derivatives of H_z at the substrate–resonator boundary, the following combination of derivative operations must be performed:

$$\frac{\partial}{\partial y} \cdot (4a) - \frac{\partial}{\partial x} \cdot (4b) \quad (5)$$

which, after changes in the order of differentiation, leads to

$$\left\{\frac{\partial}{\partial z}\left(\frac{\partial E_x}{\partial y} - \frac{\partial E_y}{\partial x}\right)\right\}_{h-} = \frac{\mu_0}{\mu}\left\{\frac{\partial}{\partial z}\left(\frac{\partial E_x}{\partial y} - \frac{\partial E_y}{\partial x}\right) + \omega\kappa\left(\frac{\partial H_x}{\partial y} - \frac{\partial H_y}{\partial x}\right)\right\}_{h+}. \quad (6)$$

The terms in parentheses can be replaced with the axial components of the fields, as they are proportional to the z-components of Faraday's and Ampere's laws, yielding

$$\left\{\frac{\partial H_z}{\partial z}\right\}_{h-} = \frac{\mu_0}{\mu}\left\{\frac{\partial H_z}{\partial z}\right\}_{h+} \quad (7)$$

where, once again, $E_z \approx 0$ was taken into account. It is important to add that the same result cannot be obtained by differentiating the boundary condition on B_z at $z = h$. The reason for this being that B_z and ***not*** $\partial B_z/\partial z$ is continuous at the boundary. It should be emphasized that the relationship stated in (7) was derived from the tangential components of the E-field and contains information on their behavior (by way of the Taylor-series expansion) at the surface of the metallic ground plane.

The corresponding boundary conditions between even derivatives of H_z (with respect to z) at $z = h$ can be derived with the help of the vector-wave equation for $\vec{E}$ and $\nabla \cdot \vec{D} = 0$, keeping in mind that under the quasi-TE mode assumption, $E_z \approx 0$. As a result, within the ferrite resonator, the coupled-wave equations for E_x and E_y are given by

$$\left\{\frac{\partial^2 E_{x,y}}{\partial x^2} + \frac{\partial^2 E_{x,y}}{\partial y^2} + \frac{\mu\mu_0}{\mu_e}\frac{\partial^2 E_{x,y}}{\partial z^2} + \frac{(-,+)j\kappa\mu_0}{\mu_e}\frac{\partial^2 E_{y,x}}{\partial z^2} + k_0^2 \varepsilon_r E_{x,y}\right\}_{h+} = 0 \quad (8)$$

where $\mu_e = \mu^2 - \kappa^2$. On the other hand, inside the isotropic dielectric substrate, the wave equations for E_x and E_y are not coupled and have the following simple forms:

$$\left\{\frac{\partial^2 E_{x,y}}{\partial x^2} + \frac{\partial^2 E_{x,y}}{\partial y^2} + \frac{\partial^2 E_{x,y}}{\partial z^2} + k_0^2 \varepsilon_{rs} E_{x,y}\right\}_{h-} = 0. \quad (9)$$

At this point, the derivatives of E_x and E_y with respect to x and y can be eliminated from (8) and (9) by recognizing that at $z = h$, both E_x and E_y are continuous, as are their transverse derivatives. As a result, the explicit relationships between the z-derivatives of E_x and E_y at the boundary can be found in (10), shown at the bottom of this page.

Next, the same set of operations as given in (5) [but with (4) replaced with (10)] are repeated to obtain (11), shown at the bottom of this page. However, since $E_z = 0$, the second term (more specifically, its derivative with respect to z) on the right-hand side of (11) vanishes. The remaining terms in the parentheses should be recognized as being proportional to H_z, which allows for rewriting (11) as

$$\left\{\frac{\partial^2 H_z}{\partial z^2}\right\}_{h-} = \left\{\frac{\mu\mu_0}{\mu_e}\frac{\partial^2 H_z}{\partial z^2} - k_0^2(\varepsilon_{rs} - \varepsilon_r)H_z\right\}_{h+}. \quad (12)$$

$$\left\{\frac{\partial^2 E_{x,y}}{\partial z^2}\right\}_{h-} = \left\{\frac{\mu\mu_0}{\mu_e}\frac{\partial^2 E_{x,y}}{\partial z^2} + \frac{(-,+)j\kappa\mu_0}{\mu_e}\frac{\partial^2 E_{y,x}}{\partial z^2} - k_0^2(\varepsilon_{rs} - \varepsilon_r)E_{x,y}\right\}_{h+} \quad (10)$$

$$\left\{\frac{\partial^2}{\partial z^2}\left(\frac{\partial E_x}{\partial y} - \frac{\partial E_y}{\partial x}\right)\right\}_{h-} = \left\{\begin{array}{l} \dfrac{\mu\mu_0}{\mu_e}\dfrac{\partial^2}{\partial z^2}\left(\dfrac{\partial E_x}{\partial y} - \dfrac{\partial E_y}{\partial x}\right) - \dfrac{j\kappa\mu_0}{\mu_e}\dfrac{\partial^2}{\partial z^2}\left(\dfrac{\partial E_x}{\partial x} + \dfrac{\partial E_y}{\partial y}\right) \\ \qquad -k_0^2(\varepsilon_{rs} - \varepsilon_r)\left(\dfrac{\partial E_x}{\partial y} - \dfrac{\partial E_y}{\partial x}\right) \end{array}\right\}_{h+} \quad (11)$$

Equations (7) and (12) can now be used to determine the higher order odd and even z-derivatives of H_z, which can be written as

$$\left\{ \begin{array}{c} \dfrac{\partial^{2n+1} H_z}{\partial z^{2n+1}} \\ \dfrac{\partial^{2n} H_z}{\partial z^{2n}} \end{array} \right\}_{h-} = (-1)^n \left\{ \sqrt[2n]{k_0^2(\varepsilon_{rs}-\varepsilon_r) - \frac{\mu\mu_0}{\mu_e}\frac{\partial^2}{\partial z^2}} \left(\begin{array}{c} \dfrac{\partial H_z}{\partial z} \\ H_z \end{array} \right) \right\}_{h+}. \quad (13)$$

When these expressions are added together, they represent the boundary conditions on E_x and E_y at $z = 0$ "translated" by way of Taylor-series expansions to $z = h$. Through the use of Maxwell's equations, this information was used to determine the appropriate boundary conditions (or GIBC's) for H_z at the substrate–resonator interface. It should be pointed out that odd and even derivatives in (13) sum up to closed-form expressions of sine and cosine functions, leading to the following final form of GIBC's for H_z:

$$\left\{ \cos\left(h\sqrt{k_0^2(\varepsilon_{rs}-\varepsilon_r) - \frac{\mu_0\mu}{\mu_e}\frac{\partial^2}{\partial z}} \right) - h\frac{\mu}{\mu_0}\frac{\partial}{\partial z} \frac{\sin\left(h\sqrt{k_0^2(\varepsilon_{rs}-\varepsilon_r) - \frac{\mu_0\mu}{\mu_e}\frac{\partial^2}{\partial z^2}} \right)}{h\sqrt{k_0^2(\varepsilon_{rs}-\varepsilon_r) - \frac{\mu_0\mu}{\mu_e}\frac{\partial^2}{\partial z^2}}} \right\} \{H_z\}_h = 0. \quad (14)$$

Note that when the same procedure is repeated for the interface between the air-gap and top end-cap of the resonator, an identical form of the GIBC will be obtained, except that h and ε_{rs} will be replaced with t and 1, respectively.

Now that the GIBC's for H_z along the axial direction have been determined, the boundary condition along the radial direction is required to complete the solution of the problem. The radial dependence of H_z inside the resonator can be determined from the following equation:

$$\frac{\partial^2 H_z}{\partial \rho^2} + \frac{1}{\rho}\frac{\partial H_z}{\partial \rho} + \left(k_0^2\varepsilon_r - \frac{\mu_0}{\mu}\beta^2 \right) H_z = 0. \quad (15)$$

It is assumed that the z-dependence is $e^{\pm j\beta(z-h)}$, the field is azimuthally symmetric and corresponds to the quasi-TE_{10} mode ($E_z \approx 0$). The solution to (15) inside and outside the resonator is given by

$$\begin{pmatrix} H_{z1}(\rho) \\ H_{z2}(\rho) \end{pmatrix} = \begin{pmatrix} J_0(\gamma\rho) \\ K_0(\alpha\rho) \end{pmatrix} \left\{ \begin{pmatrix} A_1 \\ A_2 \end{pmatrix} e^{-j\beta(z-h)} + \begin{pmatrix} B_1 \\ B_2 \end{pmatrix} e^{+j\beta(z-h)} \right\} \quad (16)$$

where $\gamma^2 = (k_0^2\varepsilon_r - \mu_0\beta^2\mu)$ and $\alpha^2 = (\beta^2 - k_0^2)$. When the continuity of H_z and E_φ at $\rho = a$ is enforced (noting that for this mode $E_\rho \approx 0$ and $H_\varphi \approx 0$), the following transcendental equation for the radial dependence of the field is obtained:

$$\frac{J_0'(\gamma a)}{\gamma J_0(\gamma a)} + \frac{K_0'(\alpha a)}{\alpha K_0(\alpha a)} = 0. \quad (17)$$

The second transcendental equation is found by applying GIBC's to H_z at $z = h$ and $h + d$ using the field expressions in (16). This leads to the following set of linear equations:

$$\begin{bmatrix} G^+_{\mathrm{serh}} & (G^+_{\mathrm{serh}})^* \\ G^+_{\mathrm{serd}}e^{-j\beta d} & (G^+_{\mathrm{serd}}e^{-j\beta d})^* \end{bmatrix} \begin{bmatrix} A_1 \\ B_1 \end{bmatrix} = \begin{bmatrix} 0 \\ 0 \end{bmatrix} \quad (18)$$

whose determinant must vanish to avoid a trivial solution. The (G^+_{serh}) term is obtained from (14) by replacing $\partial/\partial z$ with $j\beta$, while for (G^+_{serd}), h must also be replaced with t. Finally, the complete expression for the determinant of the above matrix system can be written as

$$\left\{ \cos\delta_1\cos\delta_2 - h\beta^2 t\,\frac{\mu^2\sin\delta_1\sin\delta_2}{\mu_0^2\delta_1\delta_2} \right\} \sin\beta d + \frac{\beta\mu}{\mu_0}\left\{ \frac{t\cos\delta_1\sin\delta_2}{\delta_2} + \frac{h\cos\delta_2\sin\delta_1}{\delta_1} \right\} \cos\beta d = 0 \quad (19)$$

where

$$\begin{pmatrix} \delta_1 \\ \delta_2 \end{pmatrix} = \begin{pmatrix} h\sqrt{k_0^2(\varepsilon_{rs}-\varepsilon_r) + \frac{\mu_0\mu}{\mu_e}\beta^2} \\ t\sqrt{k_0^2(1-\varepsilon_r) + \frac{\mu_0\mu}{\mu_e}\beta^2} \end{pmatrix}. \quad (20)$$

At this point, the resonant frequencies of the structure shown in Fig. 1 (or its field equivalent, shown in Fig. 2) can be determined by simultaneously solving (17) and (19).

TABLE I
VALIDATION DATA FOR THREE DIFFERENT RESONATORS.
(*NUMBERS IN PARENTHESES CORRESPOND TO GIBC APPROACH)

	a (mm)	d (mm)	f_o @ 500 Oe	f_o @ 1000 Oe	f_o @ 2000 Oe
Case 1	7.49	7.48	6.15 (6.16)*	6.50 (6.51)	6.77 (6.78)
Case 2	7.00	6.95	6.60 (6.61)	6.98 (6.98)	7.26 (7.27)
Case 3	3.85	3.41	12.63 (12.64)	13.45 (13.46)	14.07 (14.08)

III. NUMERICAL RESULTS

The resonant properties of three different resonators, whose dimensions are listed in Table I, were investigated in this paper.

The dielectric constants of the substrate and resonator were taken to be $\varepsilon_{rs} = 2.54$ and $\varepsilon_r = 15$, respectively, with the saturation magnetization of the ferrite being $4\pi M_s = 500$ G. The resonant frequencies were computed first for the quasi-TE_{10} mode of a circular ferrite post, which is an approximation to the HE_{11} mode of a ferrite rod [14]. The post is sandwiched between two infinitely large perfectly conducting plates (as in Fig. 2, with GIBC planes replaced by perfect electric conductor (PEC) planes). These results were compared to those calculated with the help of GIBC's for the resonant structure shown in Fig. 1, when both t and h are 1 μm. Since f_o for the post, whose end-caps are touching the metal plates, the resonant frequencies can be computed analytically, it serves as a validation example for the computations made with the use of GIBC's.

As can be seen from Table I, the agreement between the GIBC formulation and solution to the "shorted" post boundary-value problem (as a function of the applied bias field) is very good. The differences were typically in the third decimal place, and were rounded off for presentation. In general, the GIBC-based approach leads to higher values for f_o, which can likely be attributed to the fact that both the tuning plate and ground plane were located 1 μm from the resonator.

To illustrate the resonant behavior of ferrite substrate-mounted resonators, the resonant frequencies were calculated and plotted in Figs. 3–5 for all three resonators (cases 1–3 with h, $t = 0.7$, 0.72, 0.7, 1.25, and 0.254, 5.0 mm, respectively) as functions of the bias field for different values of the saturation magnetization $4\pi M_s$. Note that the most rapid variation in the resonant frequency occurs at low values of the biasing field, gradually approaching asymptotic values

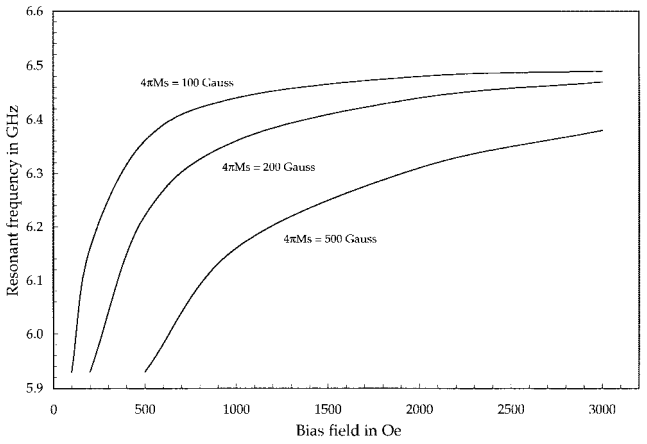

Fig. 3. Resonant frequency of the first resonator (case 1) as a function of applied bias field.

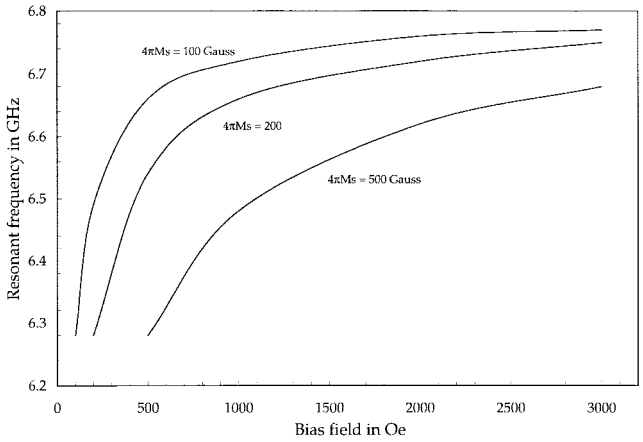

Fig. 4. Resonant frequency of the second resonator (case 2) as a function of applied bias field.

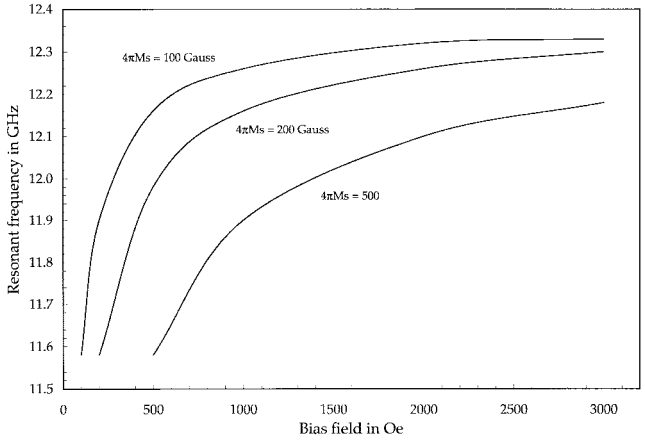

Fig. 5. Resonant frequency for the third resonator (case 3) as a function of applied bias field.

with the increasing field. In addition, the highest resonant frequencies are associated with the lowest values of $4\pi M_s$.

Next, a study was performed to assess what happens as the aspect ratio of radius-to-resonator height (a/d) changes. Fig. 6 shows the variation of the resonant frequency for the first resonator (case 1), for which the substrate thickness and displacement of the tuning plate are

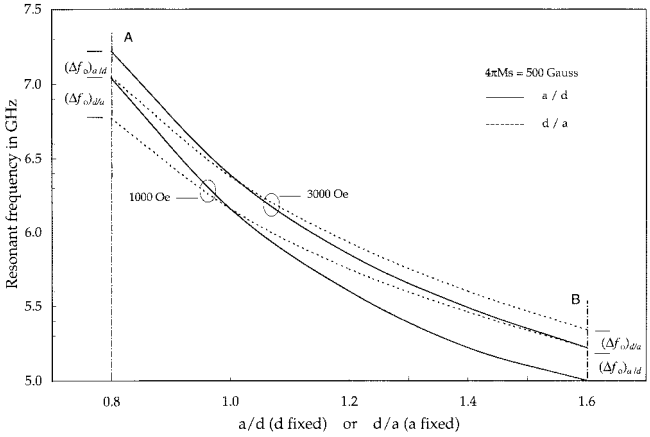

Fig. 6. Resonant frequency of the first resonator as a function of aspect ratio.

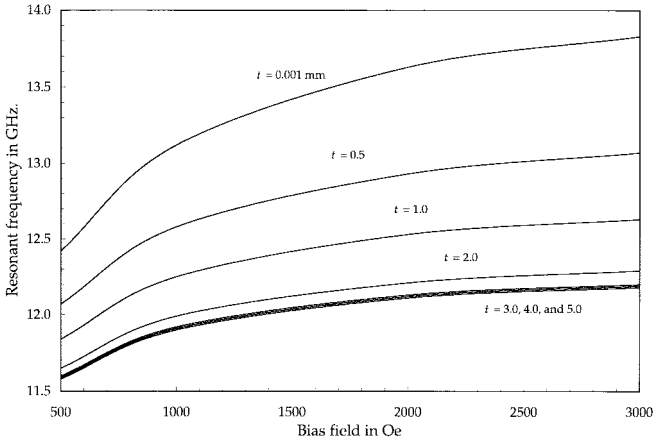

Fig. 7. Resonant frequency for the third resonator as a function of tuning plate location.

0.7 and 0.72 mm, respectively. As can be seen, the resonant frequency is more sensitive to the changes in the geometry at lower bias field values and, in general, f_o decreases as either d/a or a/d increase. It is interesting to note that the biasing field affects the change in frequency (Δf_o) differently at high and low values of the a/d and d/a ratios (see points A and B in Fig. 6).

Finally, the effect of the tuning plate on the resonator was considered. This time, the resonant frequencies of the ferrite post with smallest dimensions (case 3) were calculated as a function of the applied bias field, while the tuning plate was gradually moved further away from the resonator. The results are summarized in Fig. 7, showing that, as expected, most of the interaction between the resonator and tuning plate occurs while both are in close proximity. In addition, it is also evident that the greatest variation in f_o is associated with low values of the biasing field.

IV. Conclusion

A semianalytical approach was presented for the analysis of substrate-mounted cylindrical ferrite resonators. The use of GIBC's was utilized in problems involving magnetically anisotropic media. The approach was validated for a special geometry, having an approximate analytical solution. Numerous data were presented for ferrite resonators as function of the applied biasing field, changing geometrical dimensions, and location of the tuning plate.

REFERENCES

[1] S. B. Cohn, "Microwave bandpass filters containing high-Q dielectric resonator," *IEEE Trans. Microwave Theory Tech.*, vol. MTT-16, pp. 218–227, Apr. 1968.

[2] P. Guillon and Y. Garault, "Accurate resonant frequencies of dielectric resonators," *IEEE Trans. Microwave Theory Tech.*, vol. MTT-25, pp. 916–922, Nov. 1977.

[3] T. Itoh and R. S. Rudokas, "New methods for computing the resonant frequencies of dielectric resonators," *IEEE Trans. Microwave Theory Tech.*, vol. MTT-25, pp. 52–54 Jan. 1977.

[4] M. Jaworski and M. W. Pospieszalski, "An accurate solution of the cylinder dielectric resonator problem," *IEEE Trans. Microwave Theory Tech.*, vol. MTT-27, pp. 639–643, July 1979.

[5] A. Glisson, D. Kajfez, and J. James, "Evaluation of modes in dielectric resonators using a surface integral equation formulation," *IEEE Trans. Microwave Theory Tech.*, vol. MTT-31, pp. 1023–1029, Dec. 1983.

[6] K. A. Zaki and C. Chen, "New results in dielectric-loaded resonators," *IEEE Trans. Microwave Theory Tech.*, vol. MTT-34, pp. 815–824, July 1986.

[7] M. Yousefi, S. K. Chaudhuri, and S. Safavi-Naeini, "GIBC formulation for the resonant frequencies and field distribution of substrate-mounted dielectric resonator," *IEEE Trans. Antennas Propagat.*, vol. 42, pp. 38–46, Jan. 1994.

[8] Y. Chen *et al.*, "Tuning effects of cylindrical dielectric-loaded resonators," *Microwave Opt. Technol. Lett.*, vol. 15, no. 3, pp, 127–134, June 1997.

[9] J.-M. Guan and C.-C. Su, "Resonant frequencies and field distributions for shielded uniaxially anisotropic dielectric rod resonator by the FD-SIC method," *IEEE Trans. Microwave Theory Tech.*, vol. 45, pp. 1767–1777, Oct. 1997.

[10] R. E. Collin, *Foundations for Microwave Engineering*, 2nd ed. New York: McGraw-Hill, 1992, sec. 6.7.

[11] S. N. Karp and F. C. Karal, Jr., "Electromagnetic wave theory: Part I," in *Generalized Impedance Boundary Conditions with Application to Surface Wave Structures*, J. Brown, Ed. New York: Pergamon, 1967.

[12] H. Peng, "Study of whispering gallery models in double disk sapphire resonators," *IEEE Trans. Microwave Theory Tech.*, vol. 44, pp. 848–853, June 1996.

[13] J. Krupka, P. Blondy, D. Cros, P. Guillon, and R. G. Geyer, "Whispering gallery modes and permeability tensor measurements in magnetized ferrite resonators," *IEEE Trans. Microwave Theory Tech.*, vol. 44, pp. 1097–1102, July 1996.

[14] W. H. Von Aulock and C. E. Fay, *Linear Ferrite Devices for Microwave Applications*. New York: Academic, 1968, pp. 30–35.

Analysis of Propagation Characteristics and Field Images for Printed Transmission Lines on Anisotropic Substrates Using a 2-D-FDTD Method

Ming-sze Tong and Yinchao Chen

***Abstract*— In this paper, we apply an efficient two-dimensional (2-D) finite-difference time-domain (FDTD) algorithm onto an analysis of uniform transmission lines printed on various anisotropic substrates. By investigating the transverse resonant properties of the structures, we obtain their propagation characteristics, as well as the field images at specified frequencies. To eliminate the Gibbs phenomenon generated by a sudden time-stepping termination, we employ the Blackman–Harris window (BHW) function to truncate and modulate the entire time-domain fields, which leads to a significant time saving by comparing the conventional time-stepping termination.**

I. INTRODUCTION

The finite-difference time-domain (FDTD) method is a very powerful technique in solving the Maxwell's equations related to boundary-value problems, especially the transmission-line problems, conventionally by using three-dimensional (3-D) techniques [1]–[3]. One commonly known disadvantage of the conventional FDTD is that it requires large amounts of computer central processing unit (CPU) time and memory space to discretize all fields and medium parameters in the entire 3-D computation domain, and to iterate the FDTD algorithm until the fields stabilize. Recently, Xiao and Vahldieck presented a two-dimensional (2-D) FDTD algorithm to analyze microstrip lines, and Hofschen and Wolff improved the algorithm by using a time-domain series technique [4], [5]. Similarly, Chen and Mittra introduced the concept of transverse resonance to the FDTD for transmission-line analysis, and presented a one-dimensional (1-D) FDTD algorithm for analyzing axisymmetric waveguides [6]. In principle, these FDTD techniques are more accurate than the 3-D FDTD scheme for analyzing transmission lines since they take an advantage of the analytical nature of solutions along the longitudinal direction.

In this paper, following a similar approach used in [4]–[6], we apply an efficient 2-D FDTD algorithm onto an analysis of various transmission lines printed on anisotropic substrates. By investigating the transverse resonant properties of the structures, we obtain their propagation characteristics, as well as the field images at specified frequencies. For efficiency and accuracy, we employ the Blackman–Harris window (BHW) function to truncate and modulate the entire time-domain fields rather than following the conventional rectangular windowing time-stepping termination, which leads to a significant time saving by reducing the total number of iterations.

II. FDTD ALGORITHM AND IMPLEMENTATION

To ensure that the Maxwell's equations to be discretized are in the form of the FDTD algorithm which contains only real variables, we represent the field quantities in the form

$$\begin{bmatrix} \vec{E}(\vec{r}, t) \\ \vec{H}(\vec{r}, t) \end{bmatrix} = \begin{Bmatrix} [jE_x(x, y, t), jE_y(x, y, t), E_z(x, y, t)] \\ [H_x(x, y, t), H_y(x, y, t), jH_z(x, y, t)] \end{Bmatrix} \cdot e^{-j\beta z}. \quad (1)$$

Manuscript received July 11, 1996; revised March 2, 1998. This work was supported by the Hong Kong Polytechnic University under Grant V312.

The authors are with the Department of Electronic Engineering, Hong Kong Polytechnic University, Hong Kong.

Publisher Item Identifier S 0018-9480(98)07233-0.